www.elsevier.com/locate/jbiomech

Theoretical Effects of fully ductile versus fully brittle behaviors of bone tissue on the strength of the Human proximal femur and vertebral body

Shashank Nawathe, Haisheng Yang, Aaron J. Fields, Mary L. Bouxsein, Tony M. Keaveny

PII: S0021-9290(15)00159-1
DOI: http://dx.doi.org/10.1016/j.jbiomech.2015.02.066
Reference: BM7083

To appear in: *Journal of Biomechanics*

Received date: 28 August 2014
Revised date: 26 February 2015
Accepted date: 28 February 2015

Cite this article as: Shashank Nawathe, Haisheng Yang, Aaron J. Fields, Mary L. Bouxsein, Tony M. Keaveny, Theoretical Effects of fully ductile versus fully brittle behaviors of bone tissue on the strength of the Human proximal femur and vertebral body, *Journal of Biomechanics,* http://dx.doi.org/10.1016/j.jbiomech.2015.02.066

Theoretical Effects of Fully Ductile versus Fully Brittle Behaviors of Bone Tissue on the Strength of the Human Proximal Femur and Vertebral Body

Shashank Nawathe[1], Haisheng Yang[2], Aaron J. Fields[3], Mary L. Bouxsein[4], Tony M. Keaveny[1,5]

[1] Department of Mechanical Engineering, University of California, Berkeley, CA, USA
[2] Department of Basic Medical Sciences, Purdue University, IN, USA
[3] Department of Orthopaedic Surgery, University of California, San Francisco, CA, USA
[4] Beth Israel Deaconess Medical Center, Boston, MA, USA
[5] Department of Bioengineering, University of California, Berkeley, CA, USA

Submitted to
Journal of Biomechanics
Revision 2

Running Title: Whole-bone ductile and brittle behaviors

Funding Sources: National Science Foundation via XSEDE TG-MCA00N019

Number of words: 3401 (Introduction through Discussion, exclusive of references)

Number of Figures: 6
Number of Tables: 2 (in Appendix)

Corresponding author:
Shashank Nawathe
Department of Mechanical Engineering
University of California
Berkeley, CA 94720-1740
USA
(510) 508-1263
shashank@berkeley.edu
nawathe.shashank@gmail.com

Please address all reprint requests to:
Tony M. Keaveny
6175 Etcheverry Hall
University of California
Berkeley, CA 94720-1740
USA
(510) 642-8017, fax (510) 642-6163
tmk@me.berkeley.edu

Conflicts of Interest:
Dr. Keaveny holds equity interests in O.N. Diagnostics, LLC. The other authors do not have any conflicts of interest.

Abstract

The influence of the ductility of bone tissue on whole-bone strength represents a fundamental issue of multi-scale biomechanics. To gain insight, we performed a computational study of 16 human proximal femurs and 12 T9 vertebral bodies, comparing the whole-bone strength for the two hypothetical bounding cases of fully brittle versus fully ductile tissue-level failure behaviors, all other factors, including tissue-level elastic modulus and yield stress, held fixed. For each bone, a finite element model was generated (60–82 μm element size; up to 120 million elements) and was virtually loaded in habitual (stance for femur, compression for vertebra) and non-habitual (sideways fall, only for femur) loading modes. Using a geometrically and materially non-linear model, the tissue was assumed to be either fully brittle or fully ductile. We found that, under habitual loading, changing the tissue behavior from fully ductile to fully brittle reduced whole-bone strength by 38.3 ± 2.4% (mean ± SD) and 39.4 ± 1.9% for the femur and vertebra, respectively ($p=0.39$ for site difference). These reductions were remarkably uniform across bones, but (for the femur) were greater for non-habitual (57.1 ± 4.7%) than habitual loading ($p < 0.001$). At overall structural failure, there was 5–10-fold less failed tissue for the fully brittle than fully ductile cases. These theoretical results suggest that the whole-bone strength of the proximal femur and vertebra can vary substantially between fully brittle and fully ductile tissue-level behaviors, an effect that is relatively insensitive to bone morphology but greater for non-habitual loading.

Keywords: tissue-level ductility; femur, microstructure; whole bone; fracture

1. Introduction

The post-yield ductility of bone tissue, which is associated primarily with its organic components and enables the tissue to deform and take load beyond the elastic range, varies substantially across and within vertebrates. Bone tissue from the tympanic bulla in fin whales is highly brittle whereas bone tissue from the antler in red deer can sustain extremely large deformations before fracturing (Currey 2002); and human bone lies somewhere in between (Hernandez et al. 2005; McCalden et al. 1993; Reilly and Burstein 1975). One poorly understood issue is how tissue-level post-yield ductility *per se* influences the organ level strength of the bone — independent of other key bone-strength factors, such as bone mineral content, bone geometry, and microstructure, as well as the elastic and yield material properties of the tissue. This is a particularly challenging problem for structurally complex bones that contain both trabecular bone and thin cortices, such as the proximal femur and vertebra. From an evolutionary biomechanics perspective, understanding the relation between tissue-level post-yield ductility and whole-bone strength might provide insight into how bones evolved. This relation is also of interest clinically as tissue-level ductility can be very low in certain bone pathologies, e.g. *osteogenesis imperfecta*, and it has been proposed that subtle variations in tissue post-yield ductility may play a role in age-related bone fragility and the etiology of osteoporotic hip fractures (Ammann and Rizzoli 2003; Turner 2002).

While the relation between tissue-level post-yield ductility at one physical scale and strength of the bone at some higher scale has recently been investigated for small specimens of trabecular bone (Nawathe et al. 2013), and while this relation is relatively well understood for structurally simple diaphyseal-type bones composed only of cortical bone (Beer et al. 2006), little is known regarding the relation between whole-bone strength and tissue-level ductility in

more complex whole bones such as the proximal femur and vertebral body, nor the magnitude of this effect. This multi-scale biomechanics problem is confounded by the vast heterogeneity in whole-bone geometry and morphology across the population (Bell et al. 1999; Fazzalari et al. 2006; Keaveny et al. 2010; Mosekilde and Mosekilde 1990). Further, the interaction between the cortical and trabecular compartments and the type of external loading can alter the underlying micro-mechanics (Nawathe et al. ; Van Rietbergen et al. 2003; Verhulp et al. 2008) and therefore might mediate the relationship between tissue-level ductility and whole-bone strength.

Addressing these challenges, we utilized non-linear finite element analyses of a cohort of human proximal femurs and vertebrae to investigate how, in theory, whole-bone strength is altered when the tissue-level post-yield deformation is changed from being fully ductile to fully brittle — the two hypothetical bounds of tissue-level post-yield ductility. Computer simulations make it feasible to quantitatively assess the effects of tissue-level ductility on whole-bone strength in a precise repeated-measures manner, which is not possible solely with experimentation due to the difficulty of altering tissue-level post-yield ductility in a controlled fashion as well as the destructive nature of any physical strength testing. In this way, we provide estimates of the bounds of the influence of tissue-level post-yield ductility *per se* on whole-bone strength, accounting for most other factors that influence bone strength.

2. Materials and Methods

2.1 Specimen Preparation and Imaging

This investigation was performed on sixteen human proximal femurs (age = 76 ± 10 years, range = 62-93 years; n = 12 female, n = 4 male) and twelve thoracic ninth (T9) vertebral bodies (age = 77 ± 11 years; n= 3 female, n = 9 male) that were obtained fresh-frozen from

cadavers, with no medical history of metabolic bone disorders. High-resolution images were acquired of each intact femur (XtremeCT; isotropic voxel size of 61.5-μm, Scanco Medical AG; Brüttisellen, Switzerland) and vertebra (micro-CT, isotropic voxel size of 30-μm, Scanco Medical AG; Brüttisellen, Switzerland). Using a volume-preserving coarsening routine and a bone-specific global threshold value, the femur and vertebra images were coarsened to 82-μm and 60-μm voxel size, respectively, to facilitate computational analysis. The trabecular and cortical compartments within the whole bones were also identified (Eswaran et al. 2006; Nawathe et al. 2014) using a two-dimensional ray-based search algorithm (IDL software suite, ITT Visual Information Solutions, Boulder, CO, USA).

2.2 Finite Element Modeling

Some of the bones included in this analysis were used in previous analyses (Fields et al. 2012; Nawathe et al. 2014; Yang et al. 2012). Finite element models were created from the images by converting each coarsened image voxel directly into an 8-noded cube-shaped finite element (Van Rietbergen et al. 1995). The finite element models for the proximal femur had up to 120 million elements and those of the vertebra had up to 70 million elements. Two different types of loading conditions were implemented — one to simulate habitual loading (femur and spine) and the other non-habitual loading (femur only). For the habitual loading (Figure 1a), we used displacement boundary conditions to simulate stance loading for the femur (Keyak et al. 2001) and uniform compression for the vertebral body (Fields et al. 2012). For the non-habitual loading (Figure 1b, only performed for the femur), we simulated a 15° sideways fall on the greater trochanter (Nawathe et al. 2014). All loads were applied through a virtual layer of

polymethylmethacrylate (E = 2500 MPa) in order to distribute the loads evenly over the bone surfaces.

For both the hip and spine, all elements were assigned the same tissue-level elastic and yield properties. The isotropic elastic modulus of 7.3 GPa (Nawathe et al. 2014) was initially calibrated by comparing the finite element-estimated vs. experimental measures of femoral strength for n=12 femurs (R^2=0.94), and was then verified using n=6 additional femurs (R^2=0.92). We used a Poisson's ratio of 0.3, and yield strains of 0.81% in compression and 0.33% in tension, respectively (Bayraktar et al. 2004). For all analyses, kinematic large-deformation geometric non-linearity was included in the constitutive model (Bevill et al. 2006; Stolken and Kinney 2003). For computational efficiency, the bone tissue in the superior portion of the femoral head was not allowed to fail so as to eliminate spurious stress oscillations near the boundary conditions. For these models, we have previously reported a high correlation (R^2 = 0.94 for femurs and R^2 = 0.85 for vertebra) between the finite element-estimated and experimentally determined measures of whole-bone strength (Fields et al. 2012; Nawathe et al. 2014), which supports the validity of our modeling approach.

For each model, two separate non-linear finite element analyses were performed to simulate two hypothetical bounding cases of post-yield behavior, namely fully brittle and fully ductile tissue-level failure behaviors (Figure 2). For the fully ductile case (Figure 2a), we assumed tissue-level failure by yielding, using a rate-independent elasto-plasticity model (Papadopoulos and Lu 1998) comprised of a modified von-Mises criterion with tension-compression strength asymmetry (Bayraktar et al. 2004; Niebur et al. 2000). In this analysis, the bone tissue can only yield, it never fractures, and there is no limit on the magnitude of the post-yield tissue-level strains. For the fully brittle case (Figure 2b), tissue-level fracture is assumed to

occur once the yield stress (in either tension or compression) is exceeded. We used a quasi-nonlinear approach to simulate this type of brittle fracture. In particular, an elastic but geometrically non-linear analysis was performed to a specified level of whole-bone strain; stresses were computed at each element centroid, as was the overall structure-level reaction force at the femoral head. This reaction force was used as a single point on the overall force-deformation (strain) curve. Then the maximum and minimum principal stresses at each element centroid were checked to identify if any exceeded the assumed respective tissue-level tensile or compressive yield strengths, and if so, that element was assumed to crack or fracture — and its tensile or compressive failure mode was noted — and its elastic modulus (and thus yield strength) was reduced 100-fold for subsequent analyses. Using these reduced properties in all such "fractured" elements, a new analysis was then performed for the whole specimen, but loaded now (from zero load) to an incrementally higher structure-level strain, producing a new value for the overall structure-level reaction force. This whole process was repeated until we generated an overall structure-level force-strain curve that displayed an ultimate point, defined by a reduction in the overall structure-level reaction force.

Substantial computational infrastructure was required to perform the overall analysis. Each finite element model contained up to 400 million degrees of freedom, and was solved using an implicit, parallel finite element framework (Adams et al. 2004). Computer simulations were performed on the supercomputing resources (Stampede and Ranger) available at the Texas Advanced Computing Center (TACC). TACC Stampede system is a 10 PFLOPS (PF) Dell Linux Cluster based on 6400+ Dell PowerEdge server nodes, wherein the compute nodes are configured with two Xeon E5-2680 processors (32GB “host” memory) and one Intel Xeon Phi SE10P Coprocessor (8GB additional memory). A typical ductile and brittle analysis for the

femur during a sideways fall consumed 14 and 10 hours run time, respectively, using 2896 processors (~181 compute nodes) in parallel. Altogether for all 88 analyses, we consumed a total single-processor-equivalent CPU time of 325 years.

2.3 Outcomes and Statistical Analyses

The main quantitative outcome was the whole-bone strength. For the fully ductile analysis, the resulting "ductile strength" was defined from the computed structure-level force-strain curve using a 0.2%-offset criterion, similar to our previous studies (Fields et al. 2012; Nawathe et al. 2014). For fully brittle analysis, the resulting "brittle strength" was defined as the maximum force on the computed structure-level force-strain curve. A 0.2%-offset was not used for these analyses since the 0.2%-offset yield strain always exceeded the ultimate strain (Figure 3).

To characterize microstructural failure mechanisms, we quantified the proportion of failed tissue at the point of structure-level failure of the whole bone. The total proportion of failed tissue was defined as the number of Gauss points exceeding the assumed tissue-level failure (yield or fracture) point divided by the total number of Gauss points in the model (excluding any polymethylmethacrylate). A similar calculation was performed for each of the cortical and trabecular compartments, and for the tensile and compressive failure modes. In the ductile analysis, the simulated tissue failure occurred via *yielding* whereas in the brittle analysis, tissue failure occurred via *fracture*. Heretofore, we use the single term '*failed tissue*' to denote failure by either yielding or fracture.

Regression analysis was used to determine the correlation between the brittle and ductile strength values. Since the sample size was small, the Mann-Whitney non-parametric U-test was performed to access the effect of anatomic site (femur versus vertebra) and loading configuration

(sideways fall versus stance) on the ratio of brittle to ductile strength, the relative amount of cortical versus trabecular tissue failure, and the relative amount of tensile versus compressive tissue failure. All statistical tests (JMP 10; SAS Institute, Cary, NC USA) were considered significant at $p < 0.05$.

3. Results

For habitual loading, changing the assumed tissue-level failure behavior from fully ductile to fully brittle substantially reduced whole-bone strength for all the femurs and vertebrae (Figure 4). On average, the whole-bone strength was reduced by 38.3 ± 2.4% (mean ± SD) and 39.4 ± 1.9% for the femur and vertebra, respectively. As a consequence, the ratio of brittle-to-ductile strength was 0.62 ± 0.02 for the femur and 0.61 ± 0.02 for the vertebra. Reflecting the substantial heterogeneity of the bones in the cohort, the ductile strength spanned a large range, the weakest bone at either site being approximately 5-fold weaker than the strongest bone (Figure 4). As reflected by the small standard deviation, the effect size was relatively uniform across all bones regardless of bone strength ($p=0.49$ for femur, $p=0.38$ for vertebra) or anatomic site ($p = 0.39$). Further, there was no significant correlation between the brittle-ductile strength ratio and such various quantitative measures of bone morphology as cortical and trabecular mass and various geometry measures (see Table A1, A2 in Appendix).

For non-habitual loading of the hip, varying the tissue-level failure behavior from fully ductile to fully brittle reduced whole-bone strength by 57.1 ± 4.7%, and the ratio of brittle to ductile strength was 0.43 ± 0.05 (Figure 4). This effect was also remarkably uniform across bones regardless of bone strength ($p = 0.12$), but was greater for non-habitual loading of the femur compared to habitual loading ($p<0.0001$).

Changing the tissue-level failure behavior from fully ductile to fully brittle also altered the microstructural failure mechanisms, different effects being observed for the femur and vertebra. The amount of failed tissue that led to structure-level failure of the bone was, on average, five-fold lower for the femurs and ten-fold lower for the vertebrae for the fully brittle compared to the fully ductile behaviors (Figure 5). The locations of tissue-level failure for the fully ductile behavior subsumed the locations of tissue-level failure for the fully brittle behavior (Figure 6). Computing the amount of failed tissue in the cortical and trabecular compartments (Figure 5a) revealed that, after changing the tissue from fully ductile to fully brittle, the relative amount of trabecular versus cortical tissue failure remained unaltered in the femur, both for a sideways fall and stance loading ($p > 0.05$ for both), but increased four-fold in the vertebra ($p < 0.0001$). Evaluating the mode (tension vs. compression) of tissue-level failure (Figure 5b) demonstrated that, after changing the tissue from fully ductile to fully brittle, the relative amount of tensile versus compressive failure increased significantly in the femur (2.5-fold increase for fall; $p < 0.0001$, and 1.5-fold increase for stance; $p = 0.001$), but was unaltered in the vertebra ($p > 0.05$).

4. Discussion

These computational results provide quantitative theoretical bounds on the expected effects of extreme variations in tissue-level bone post-yield ductility on whole-bone strength for the human proximal femur and vertebral body. The simulations revealed a large effect size — for habitual loading, whole-bone strength at both the femur and vertebra was reduced by approximately 40% when the post-yield behavior of the tissue was changed from being fully ductile to fully brittle. Surprisingly, this effect did not depend on any aspect of the bone

morphology, at either the organ or microstructural levels, despite the large variation in bone morphology across all the entire sample. We note that all other aspects of the bones were held fixed in these controlled parameter studies, including the values of tissue-level elastic modulus and yield properties. Thus, these biomechanical effects are due only to changes in the post-yield deformation of the bone tissue. Despite this uniformity of effect size, we also found that the nature of external loading on the femur was important, the effect size being greater for non-habitual loading. Mechanistically, failure at the whole-bone level required five- to ten-fold less tissue to fail when the tissue-level post-yield behavior was changed from fully ductile to fully brittle. This finding indicates that the whole bone is substantially strengthened when the underlying tissue is more ductile because increased ductility enables initially yielded bone tissue to continue to support the external loads thus enabling other trabeculae to also take appreciable load. Conversely, with fully brittle bone tissue, many of the latter trabeculae cease to contribute to overall load bearing because overall structure failure quickly occurs after fracture of the initially failed tissue and the lack of alternative viable load paths. While some of these qualitative trends might be expected, most of the results were unexpected and therefore provide new insight: the large magnitude of the effect size, its uniformity with respect to very large variations in bone morphology, and its dependence on the nature of loading at the hip. Taken together, these theoretical results suggest that the whole-bone strength of the proximal femur and vertebra can vary substantially between fully brittle and fully ductile tissue-level post-yield behaviors, an effect that is relatively insensitive to bone morphology but larger for non-habitual loading.

One finding potentially relevant to evolutionary biomechanics is the uniformity in the role of tissue-level post-yield ductility on whole-bone strength, independent of the effects of bone morphology. This finding suggests that increasing ductility at the tissue level can be a

robust mechanism to enhance whole-bone strength in trabeculated bones in vertebrates. This robustness is potentially significant since it indicates that if this mechanism were invoked as an evolutionary strategy, it would reliably deliver its intended strength-enhancing effect regardless of the particular morphology of the bone. Thus, trabeculated bones in vertebrates may have evolved in such a manner that, if weight is premium, maximizing tissue-level ductility becomes an effective and robust way to increase bone strength appreciably without needing to add mineral or mass. Since the variation in ductility in real vertebrates is less than the hypothetical extreme cases of fully brittle and fully ductile as simulated in this study, the strength advantages afforded by any such real adaptations will be lower than predicted here.

One finding potentially relevant to clinical biomechanics is the large effect size, of up to 40% for habitual loading and 60% for non-habitual loading. This effect size might apply directly to individuals having brittle-related bone pathologies such as *osteoporosis imperfacta* (Carriero et al. 2014). Recently, it was demonstrated using clinical-resolution finite element analysis that vertebral strength in adults with *osteoporosis imperfacta* increased by 15% following 18-month teriparatide treatment (Orwoll et al. 2014). While our new results do not pertain to those treatment effects, they do help further interpret those clinical results by suggesting that absolute values of strength in such individuals may be substantially lower than when assuming normal bone tissue. Of course since our simulations only addressed the extreme post-yield behaviors of the tissue, our results cannot be used to estimate how typical real variations in tissue-level post-yield ductility might play a role in the etiology of age-related fractures, nor on treatments used to reduce the risk of such fractures. Even so, since the computed effect size in our study was large, our results suggest that further research is indeed warranted to further pursue this potentially important etiological factor. Since we found that the role of tissue-level ductility did not depend

on bone morphology, consistent with our previous study on specimens of trabecular bone (Nawathe et al. 2013), any future theoretical work in this area should not require large sample sizes to gain useful insight.

The trends found here reflect underlying differences in the load sharing between the cortical and trabecular compartments and between the hip (Nawathe et al. 2015 ; Van Rietbergen et al. 2003; Verhulp et al. 2008) and spine (Eswaran et al. 2006) and the associated micromechanics. The principles of multi-scale mechanics dictate that the absolute quantity of strength-determining, load-bearing tissue in the proximal femur or vertebral body is determined by both bone mass and the extent to which the tissue can deform beyond the tissue-level elastic range without fracturing or developing appreciable cracking or damage. Our results demonstrated that the tensile and compressive failure modes of the tissue as well as the distribution of cortical versus trabecular failure were altered by both the external loading mode and the extent of tissue-level post-yield ductility. Failure of the endplates and adjacent trabecular tissue appears to dominate the initial failure mechanisms of the vertebral body (Eswaran et al. 2007; Fields et al. 2012; Yang et al. 2012), and, except in the very weakest of femurs for which failure of trabecular tissue appears to dominate (Nawathe et al. 2014), failure of both the cortical and trabecular tissue is also important during initial failure of the proximal femur, for both stance (Figure 6) and a sideways fall loading (Nawathe et al. 2014). Therefore, in any future studies that seek to further investigate the relation between tissue-level post-yield ductility and whole-bone strength, it might be important to distinguish between cortical and trabecular ductility since it appears, albeit from limited data, that real trabecular tissue is substantially more ductile than cortical tissue (Carretta et al. 2013; Hernandez et al. 2005; McCalden et al. 1993).

Our analysis has a number of limitations. First, as noted above, we did not explore the influence of typical population-variations in ductility, nor did we independently alter cortical versus trabecular ductility. Second, we used a quasi-nonlinear approach instead of a combined fracture-damage constitutive model (Harrison et al. 2013) to simulate tissue fracture. While such combined constitutive models are relatively sophisticated, their implementation in micro-CT-based whole-bone models might lead to convergence issues and it is not clear that they would have provided any additional insight in this particular study since our approach captured the dominant physics of brittle fracture. Lastly, our results have not yet been validated by experiments. Such direct validation is not only technically challenging but may not even be feasible in any type of experimental study utilizing either cadaver or animal models due to the challenge of selectively altering only the tissue-level post-yield ductility, keeping all other tissue elastic and yield material properties intact. Thus, our approach, which provides only theoretical bounds on expected behavior, nevertheless provides unique qualitative and quantitative insight into what is otherwise a largely intractable biomechanics problem.

Acknowledgements

Computational resources were made available through the National Science Foundation via XSEDE (Grant TG-MCA00N019). We thank Dr. Michael Liebschner for imaging the vertebrae.

Appendix:

We determined the correlations between the ratio of brittle to ductile strength and the selected measures of bone morphology, for both femurs and vertebra. Standard measures of bone volume and geometry were derived from the original micro-CT scans of the bones. These measures have been described previously (Carpenter et al. 2005; Eswaran et al. 2006; Gregory et al. 2008; Nawathe et al. 2014; Shi et al. 2009). The correlations between the brittle-to-ductile strength ratio and the measures of bone volume and geometry were not statistically significant ($p>0.05$), both for femurs (Table A1) and vertebrae (Table A2). This finding suggests that the effect of tissue-level failure behavior on whole-bone strength depends little on the bone morphology.

Table A1: Characteristics of the study population (mean, standard deviation) for the femurs (n=16) and correlation coefficients between selected outcomes and the brittle-to-ductile strength, both for a sideways fall and stance loading of the femurs. Brittle-to-ductile strength refers to the ratio of the brittle to ductile strengths of the femurs.

Outcomes and Variables (units)	Sample Characteristics (n = 16)		Brittle-to-Ductile Strength	
			Stance Load	Sideways Fall Load
	Mean	SD	*Pearson correlation coefficient (r)*	
Brittle-to-ductile strength femur stance	0.62	0.02	**1.00**	0.24
Brittle-to-ductile strength femur fall	0.43	0.04	0.24	**1.00**
Ductile strength stance (kN)	7.72	2.23	0.16	0.40
Ductile strength fall (kN)	2.62	1.02	0.03	0.31
Morphology parameters				
Total hip integral bone volume (cm^3)	42.8	8.31	0.01	0.10
Total hip cortical bone volume (cm^3)	17.3	3.68	0.11	-0.01
Total hip trab bone volume (cm^3)	25.5	5.34	-0.07	0.15
Femoral neck integral volume (cm^3)	7.93	2.16	0.53	0.28
Femoral neck cortical volume (cm^3)	3.28	0.99	0.47	0.06
Femoral neck trab volume (cm^3)	4.64	1.46	0.47	0.37
Trochanter integral volume (cm^3)	21.5	4.71	-0.30	0.11
Trochanter cortical volume (cm^3)	11.3	2.51	-0.12	0.06
Trochanter trabecular volume (cm^3)	10.2	2.70	-0.41	0.14
Total hip trab/cortical volume ratio	1.49	0.26	-0.22	0.16
Femoral neck trab/cort volume ratio	1.45	0.33	0.05	0.20
Trochanter trab/cortical volume ratio	0.91	0.20	-0.36	0.16
Geometry parameters				
Head diameter (cm)	2.21	0.13	-0.30	-0.15
Neck-axis length (cm)	6.24	4.05	0.25	-0.01
Neck-shaft angle (degrees)	126	5.13	0.35	-0.14
Neck cross-sectional area (cm^2)	7.10	1.14	0.05	-0.18
Neck areal moment of inertia (cm^4)	4.57	1.66	0.05	-0.15

Bolded values have $p < 0.05$. SD: standard deviation. $r = 0.64$ is the statistical significant limit.

Table 2: Characteristics of the study population (mean, standard deviation) for the vertebrae (n=12) and correlation coefficients between selected outcomes and the brittle-to-ductile strength for uniaxial compression loading of the vertebra. Brittle-to-ductile strength refers to the ratio of the brittle to ductile strengths of the vertebrae.

Outcomes and Variables (units)	Sample Characteristics (n = 12)		Brittle-to-Ductile Strength
	Mean	SD	*Pearson correlation coefficient (r)*
Brittle-to-ductile strength	0.61	0.02	**1.00**
Ductile strength (kN)	5.06	1.97	-0.29
Morphology parameters			
Total spine integral bone volume (cm^3)	4.82	1.33	-0.42
Total spine cortical bone volume (cm^3)	0.65	0.18	-0.49
Total spine trab bone volume (cm^3)	2.29	0.72	-0.42
Total spine trab/cortical volume ratio	3.58	1.04	-0.05
Vertical BV/TV	0.08	0.02	-0.32
Cortical thickness (mm)	0.42	0.09	-0.55
Geometry parameters			
Curvature (degree)	18.2	4.89	-0.21
Mid-sagittal cross-sectional area (cm^2)	1.79	0.49	-0.36

Bolded values have $p < 0.05$. SD: standard deviation. $r = \pm 0.59$ is the statistical significant limit.

References

Adams, M. F., Bayraktar, H. H., Keaveny, T. M. and Papadopoulos, P. (2004). Ultrascalable implicit finite element analyses in solid mechanics with over a half a billion degrees of freedom. ACM/IEEE Proceedings of SC2004: High Performance Networking and Computing.

Ammann, P. and Rizzoli, R. (2003). Bone strength and its determinants. Osteoporos Int **14 Suppl 3**: S13-18.

Bayraktar, H. H., Morgan, E. F., Niebur, G. L., Morris, G. E., Wong, E. K. and Keaveny, T. M. (2004). Comparison of the elastic and yield properties of human femoral trabecular and cortical bone tissue. J Biomech **37**(1): 27-35.

Beer, F. P., Johnston, E. R. and DeWolf, J. T. (2006). Mechanics of materials. Boston, McGraw-Hill Higher Education.

Bell, K. L., Loveridge, N., Power, J., Garrahan, N., Meggitt, B. F. and Reeve, J. (1999). Regional differences in cortical porosity in the fractured femoral neck. Bone **24**(1): 57-64.

Bevill, G., Eswaran, S. K., Gupta, A., Papadopoulos, P. and Keaveny, T. M. (2006). Influence of bone volume fraction and architecture on computed large-deformation failure mechanisms in human trabecular bone. Bone **39**(6): 1218-1225.

Carpenter, R. D., Beaupre, G. S., Lang, T. F., Orwoll, E. S. and Carter, D. R. (2005). New QCT analysis approach shows the importance of fall orientation on femoral neck strength. J Bone Miner Res **20**(9): 1533-1542.

Carretta, R., Stussi, E., Muller, R. and Lorenzetti, S. (2013). Within subject heterogeneity in tissue-level post-yield mechanical and material properties in human trabecular bone. J Mech Behav Biomed Mater **24**: 64-73.

Carriero, A., Zimmermann, E. A., Paluszny, A., Tang, S. Y., Bale, H., Busse, B., Alliston, T., Kazakia, G., Ritchie, R. O. and Shefelbine, S. J. (2014). How tough is brittle bone? Investigating osteogenesis imperfecta in mouse bone. J Bone Miner Res **29**(6): 1392-1401.

Currey, J. D. (2002). Bones — Structure and Mechanics. Princeton, New Jersey, Princeton University Press**:** 124-138.

Eswaran, S. K., Gupta, A., Adams, M. F. and Keaveny, T. M. (2006). Cortical and trabecular load sharing in the human vertebral body. J Bone Miner Res **21**(2): 307-314.

Eswaran, S. K., Gupta, A. and Keaveny, T. M. (2007). Locations of bone tissue at high risk of initial failure during compressive loading of the human vertebral body. Bone **41**(4): 733-739.

Fazzalari, N. L., Parkinson, I. H., Fogg, Q. A. and Sutton-Smith, P. (2006). Antero-postero differences in cortical thickness and cortical porosity of T12 to L5 vertebral bodies. Joint Bone Spine **73**(3): 293-297.

Fields, A. J., Nawathe, S., Eswaran, S. K., Jekir, M. G., Adams, M. F., Papadopoulos, P. and Keaveny, T. M. (2012). Vertebral fragility and structural redundancy. J Bone Miner Res **27**(10): 2152-2158.

Gregory, C. O., Corvalan, C., Ramirez-Zea, M., Martorell, R. and Stein, A. D. (2008). Detection of cardio-metabolic risk by BMI and waist circumference among a population of Guatemalan adults. Public Health Nutr **11**(10): 1037-1045.

Harrison, N. M., McDonnell, P., Mullins, L., Wilson, N., O'Mahoney, D. and McHugh, P. E. (2013). Failure modelling of trabecular bone using a non-linear combined damage and fracture voxel finite element approach. Biomech Model Mechanobiol **12**(2): 225-241.

Hernandez, C. J., Tang, S. Y., Baumbach, B. M., Hwu, P. B., Sakkee, A. N., van der Ham, F., DeGroot, J., Bank, R. A. and Keaveny, T. M. (2005). Trabecular microfracture and the influence of pyridinium and non-enzymatic glycation-mediated collagen cross-links. Bone **37**(6): 825-832.

Keaveny, T. M., Kopperdahl, D. L., Melton, L. J., 3rd, Hoffmann, P. F., Amin, S., Riggs, B. L. and Khosla, S. (2010). Age-dependence of femoral strength in white women and men. J Bone Miner Res **25**(5): 994-1001.

Keyak, J. H., Skinner, H. B. and Fleming, J. A. (2001). Effect of force direction on femoral fracture load for two types of loading conditions. J Orthop Res **19**(4): 539-544.

McCalden, R. W., McGeough, J. A., Barker, M. B. and Court-Brown, C. M. (1993). Age-related changes in the tensile properties of cortical bone. The relative importance of changes in porosity, mineralization, and microstructure. J Bone Joint Surg Am **75**(8): 1193-1205.

Mosekilde, L. and Mosekilde, L. (1990). Sex differences in age-related changes in vertebral body size, density and biomechanical competence in normal individuals. Bone **11**(2): 67-73.

Nawathe, S., Akhlaghpour, H., Bouxsein, M. L. and Keaveny, T. M. (2014). Microstructural failure mechanisms in the human proximal femur for sideways fall loading. J Bone Miner Res **29**(2): 507-515.

Nawathe, S., Juillard, F. and Keaveny, T. M. (2013). Theoretical bounds for the influence of tissue-level ductility on the apparent-level strength of human trabecular bone. J Biomech **46**(7): 1293-1299.

Nawathe, S., Nguyen, B. P., Barzanian, N., Akhlaghpour, H., Bouxsein, M. L. and Keaveny, T. M. Cortical and trabecular load sharing in the human femoral neck. Journal of Biomechanics (2015), http://dx.doi.org/10.1016/j.jbiomech.2014.12.022.

Niebur, G. L., Feldstein, M. J., Yuen, J. C., Chen, T. J. and Keaveny, T. M. (2000). High-resolution finite element models with tissue strength asymmetry accurately predict failure of trabecular bone. Journal of Biomechanics **33**: 1575-1583.

Orwoll, E. S., Shapiro, J., Veith, S., Wang, Y., Lapidus, J., Vanek, C., Reeder, J. L., Keaveny, T. M., Lee, D. C., Mullins, M. A., Nagamani, S. C. and Lee, B. (2014). Evaluation of teriparatide treatment in adults with osteogenesis imperfecta. J Clin Invest **124**(2): 491-498.

Papadopoulos, P. and Lu, J. (1998). A general framework for the numerical solution of problems in finite elasto-plasticity. Computer Methods in Applied Mechanics and Engineering **159**(1-2): 1-18.

Reilly, D. T. and Burstein, A. H. (1975). The elastic and ultimate properties of compact bone tissue. J Biomech **8**(6): 393-405.

Shi, X., Wang, X. and Niebur, G. L. (2009). Effects of loading orientation on the morphology of the predicted yielded regions in trabecular bone. Ann Biomed Eng **37**(2): 354-362.

Stolken, J. S. and Kinney, J. H. (2003). On the importance of geometric nonlinearity in finite-element simulations of trabecular bone failure. Bone **33**(4): 494-504.

Turner, C. H. (2002). Determinants of skeletal fragility and bone quality. J Musculoskelet Neuronal Interact **2**(6): 527-528.

Van Rietbergen, B., Huiskes, R., Eckstein, F. and Ruegsegger, P. (2003). Trabecular bone tissue strains in the healthy and osteoporotic human femur. Journal of Bone and Mineral Research **18**(10): 1781-1788.

Van Rietbergen, B., Weinans, H., Huiskes, R. and Odgaard, A. (1995). A new method to determine trabecular bone elastic properties and loading using micromechanical finite element models. Journal of Biomechanics **28**(1): 69-81.

Verhulp, E., van Rietbergen, B. and Huiskes, R. (2008). Load distribution in the healthy and osteoporotic human proximal femur during a fall to the side. Bone **42**(1): 30-35.

Yang, H., Nawathe, S., Fields, A. J. and Keaveny, T. M. (2012). Micromechanics of the human vertebral body for forward flexion. J Biomech **45**(12): 2142-2148.

Figure Captions

Figure 1: Boundary conditions used to simulate: a) habitual loading, for the femurs and vertebrae, and b) non-habitual loading, only for the femurs. Habitual loading: stance loading of the femur and uniaxial compression loading of the vertebra; non-habitual loading: a sideways fall on the greater trochanter of the femur. A virtual layer of polymethyl methacrylate (PMMA; E = 2,500 MPa) was used to distribute loads evenly.

Figure 2: Material constitutive model for the bone tissue, depicting the stress–strain response at the tissue-level for: a) fully brittle, and b) fully ductile bone tissue. The same elastic modulus and yield strains (and yield stresses) was used in all cases, the only variable being the amount of post-yield deformation (either none for the brittle case, or unlimited for the ductile case).

Figure 3: An example of a typical computed whole-bone force-deformation curve for one femur, showing the fully ductile and fully brittle behaviors and definitions of the strength for each case. The force is the total force applied to the femoral head, and the structure-level strain is the percentage change in medial-lateral width of the proximal femur when the force is applied. The general shape of these curves did not depend on the anatomic site or the loading configuration.

Figure 4: Variation in the ratio of whole-bone brittle to ductile strength across the specimens.

Figure 5: Proportion of failed tissue when the tissue-level behavior is changed from fully ductile (D) to fully brittle (B), for the femurs (n=16) for fall and stance loading and for the vertebrae

(n=12) for compression loading. The proportion of failed tissue is the amount of failed tissue in a model divided by the total amount of tissue in the model. Each bar denotes the overall mean of the proportion of failed tissue across all models, the error bars denoting the 95% confidence intervals. The shading shows either how much of the failure occurs in the cortical versus trabecular bone (a) or how much failure is due to a tensile or compressive failure mode (b).

Figure 6: A mid-frontal section of one proximal femur and a mid-sagittal section of one vertebra, showing regions of failed tissue at the overall strength point for the fully brittle and fully ductile simulations (colors depict failure mode: blue—compression; red—tension; grey—no failure). Bone strength values for this particular bone are shown in Newton (N) and the total amount of failed tissue is shown as a percentage of the total amount of tissue in the model. For numerical modeling reasons, failure was not allowed to occur in the femoral head regions of the models.

Figure 1

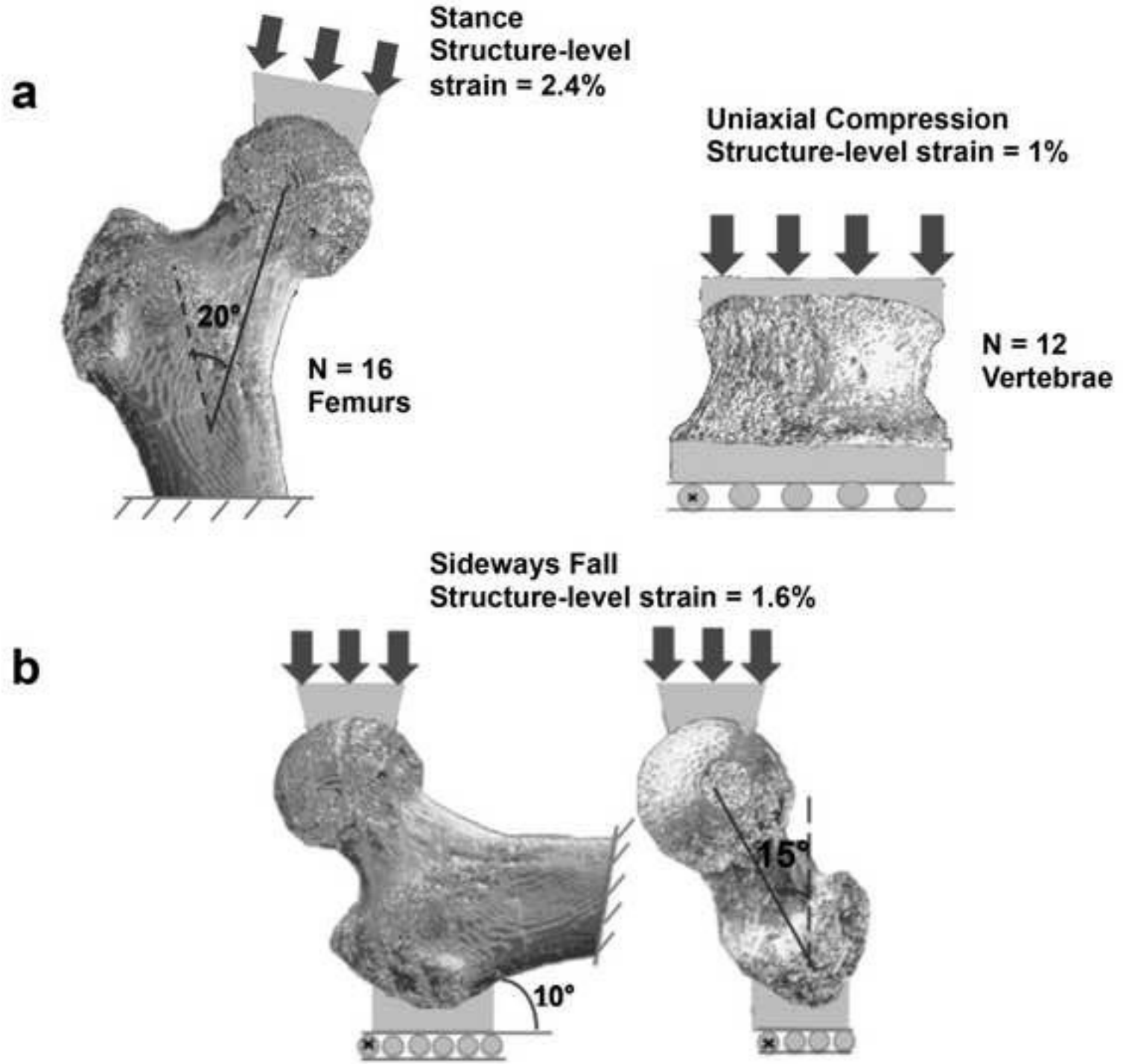

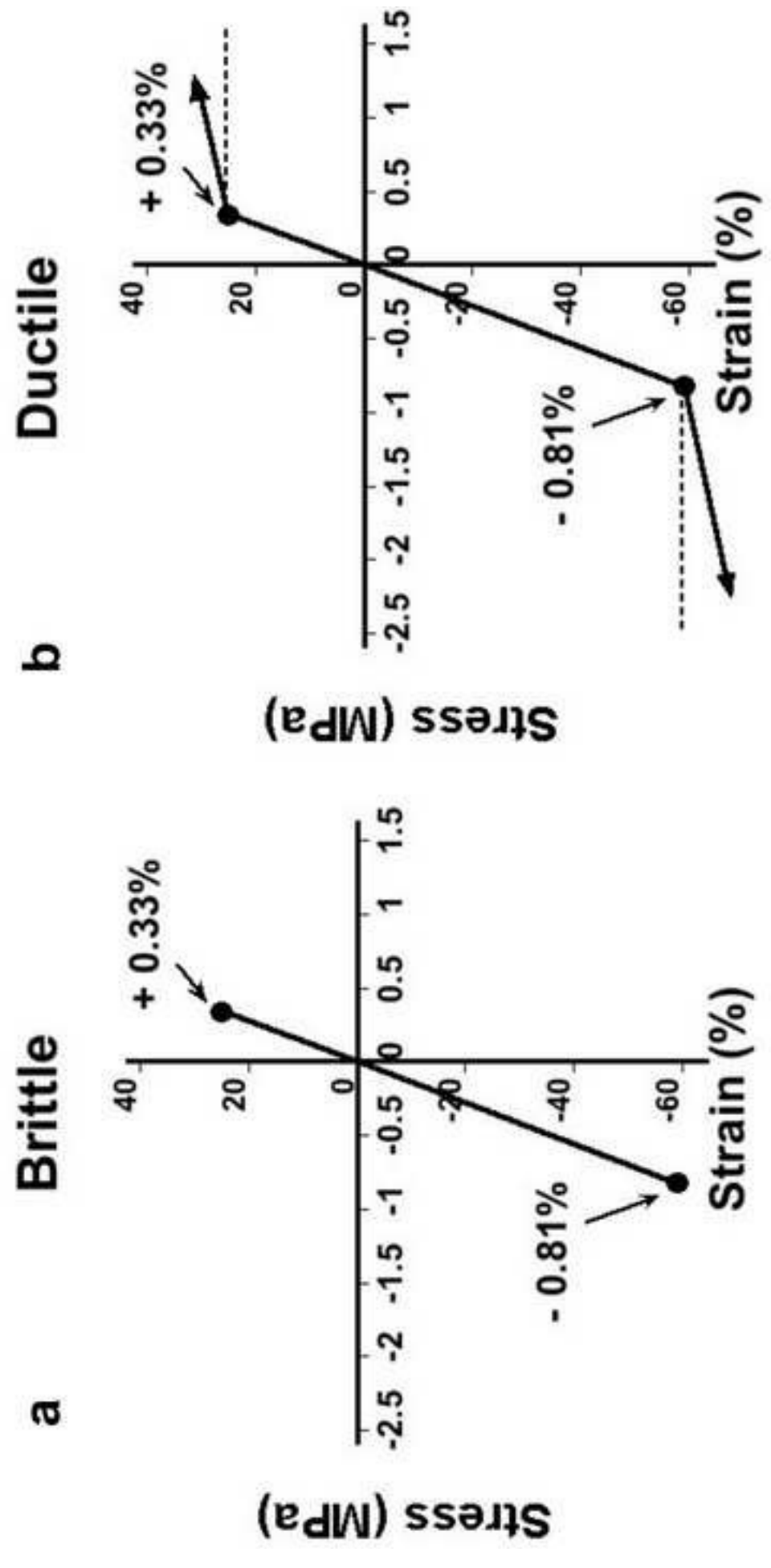
a
Brittle
b
Ductile
Stress (MPa)
Strain (%)
+ 0.33%
- 0.81%
40
20
0
-20
-40
-60
-2.5
-2
-1.5
-1
-0.5
0
0.5
1
1.5

Figure 2

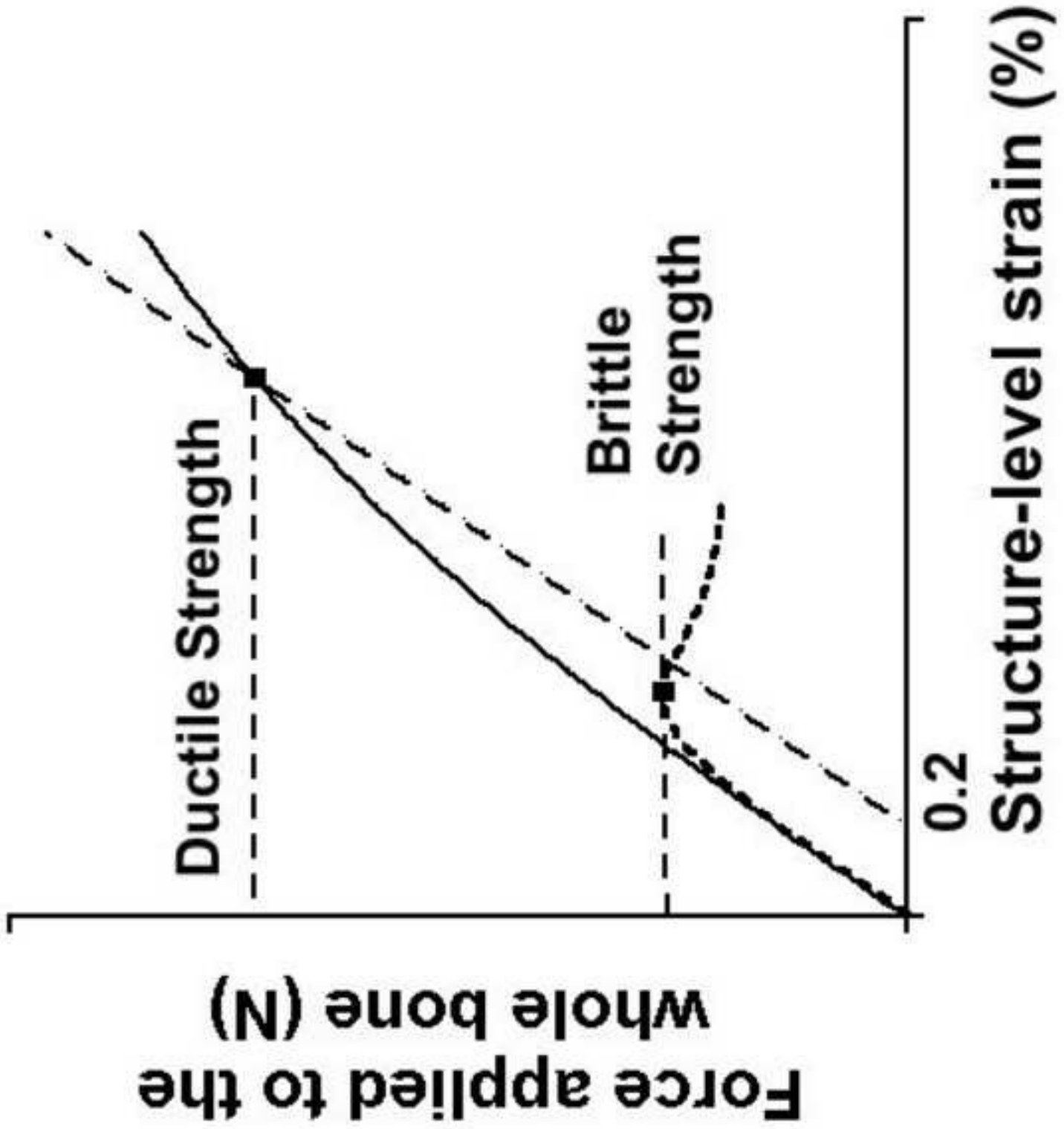

Figure 3

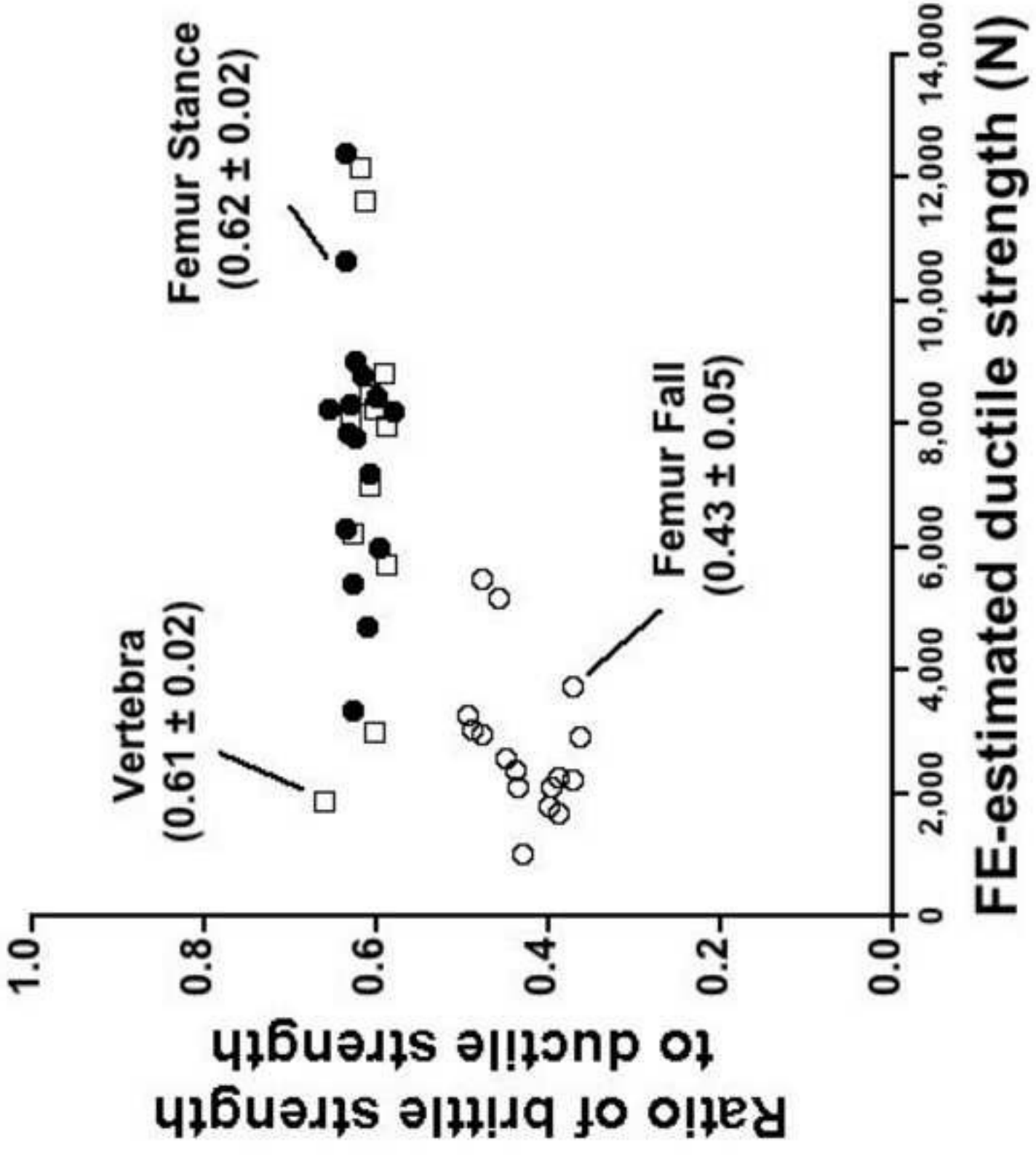
Ratio of brittle strength to ductile strength
1.0
0.8
0.6
0.4
0.2
0.0
0
2,000
4,000
6,000
8,000
10,000
12,000
14,000
FE-estimated ductile strength (N)
Vertebra
(0.61 ± 0.02)
Femur Stance
(0.62 ± 0.02)
Femur Fall
(0.43 ± 0.05)

Figure 4

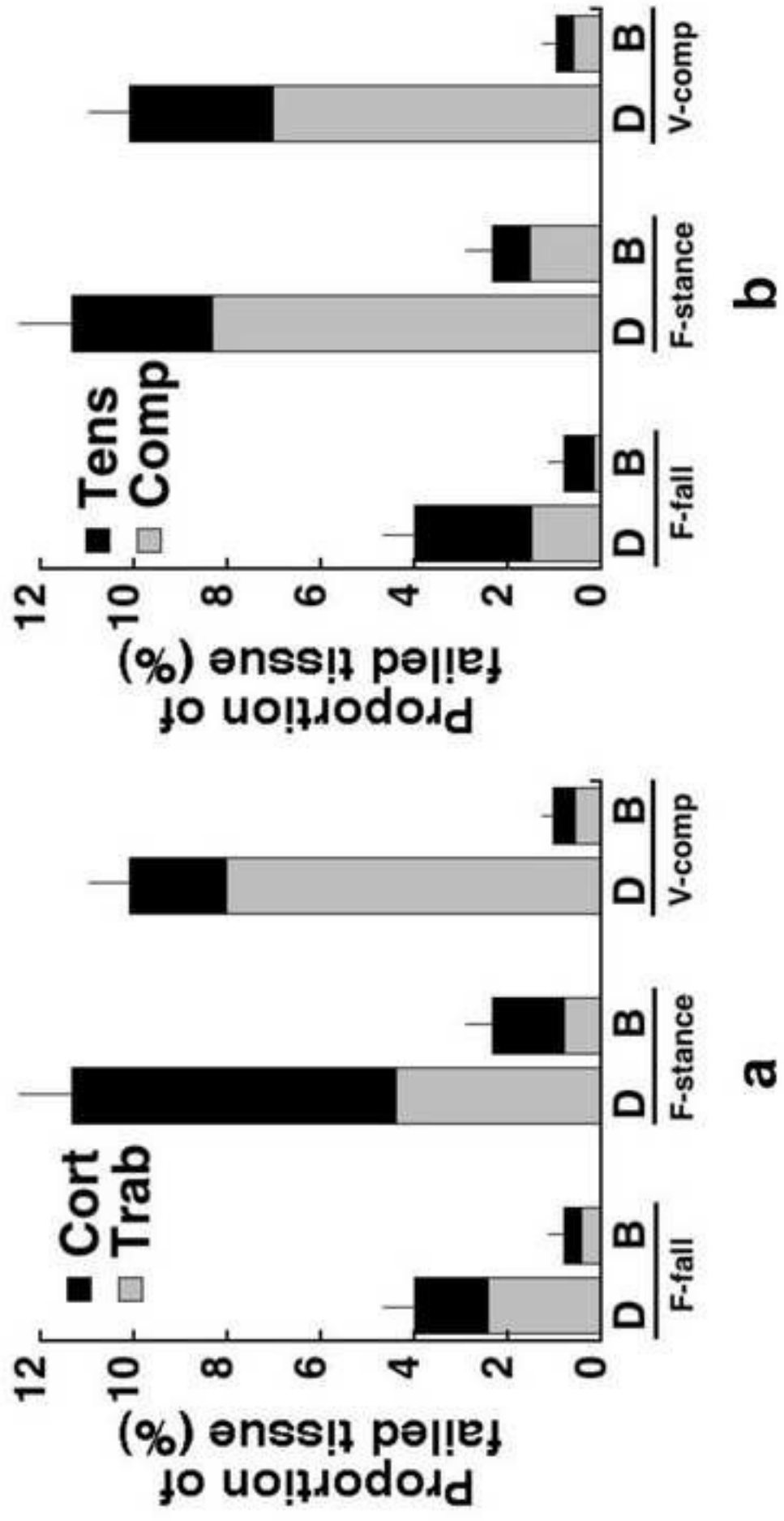
Proportion of failed tissue (%)
12
10
8
6
4
2
0
Cort
Trab
D B
F-fall
D B
F-stance
D B
V-comp
a
Tens
Comp
D B
F-fall
D B
F-stance
D B
V-comp
b

Figure 5

Figure 6